Title

Impact of atmospheric dryness on solar-induced chlorophyll fluorescence: Tower-based observations at a temperate forest

Authors

Yi, Koong
Li, Rong
Scanlon, Todd M
et al.

Publication Date

2024-05-01

DOI

10.1016/j.rse.2024.114106

Peer reviewed

Title

Impact of atmospheric dryness on solar-induced chlorophyll fluorescence: tower-based observations at a temperate forest

Authors

Koong Yi[1,2], Rong Li[1], Todd M. Scanlon[1], Manuel T. Lerdau[1], Joseph A. Berry[3], and Xi Yang[1]

Affiliations

[1]Department of Environmental Sciences, University of Virginia, Charlottesville, VA 22904, USA.

[2]Earth and Environmental Sciences Area, Lawrence Berkeley National Laboratory, CA 94720, USA.

[3]Department of Global Ecology, Carnegie Institution for Science, Stanford, CA 94305, USA.

Corresponding Authors

Koong Yi (koongyi@gmail.com)

Xi Yang (xiyang@virginia.edu)

Abstract

Solar-induced chlorophyll fluorescence (SIF) is widely accepted as a proxy for gross primary productivity (GPP). Among the various SIF measurements, tower-based SIF measurements allow for continuous monitoring of SIF variation at a canopy scale with high temporal resolution, making it suitable for monitoring highly variable plant physiological responses to environmental changes. However, because of the strong and close relationship between SIF and absorbed photosynthetically active radiation (aPAR), it may be difficult to detect the influence of environmental drivers other than light conditions. Among the drivers, atmospheric dryness (vapor pressure deficit, VPD) is projected to increase as drought becomes more frequent and severe in the future, negatively impacting plants. In this study, we evaluated the tower-based high-frequency SIF measurement as a tool for detecting plant response to highly variable VPD. The study was performed in a mixed temperate forest in Virginia, USA, where a 40-meter-tall flux tower has been measuring gas and energy exchanges and ancillary environmental drivers, and the Fluospec 2 system has been measuring SIF. We show that a proper definition of light availability to vegetation can reproduce SIF response to changing VPD that is comparable to GPP response as estimated from eddy covariance measurement: GPP decreased with rising VPD regardless of how aPAR was defined, whereas SIF decreased only when aPAR was defined as the PAR absorbed by chlorophyll ($aPAR_{chl}$) or simulated by a model (Soil Canopy Observation, Photochemistry and Energy fluxes, SCOPE). We simulated the effect of VPD on SIF with two different simulation modes of fluorescence emission representing contrasting moisture conditions, 'Moderate' and 'Soil Moisture (SM) Stress' modes. The decreasing SIF to rising VPD was only found in the SM Stress mode, implying that the SIF-VPD relationship depends on soil moisture conditions. Furthermore, we observed a similar response of SIF to VPD at hourly and daily scales, indicating that satellite measurements can be used to study the effects of environmental drivers other than light conditions. Finally, the definition of aPAR emphasizes the importance of canopy structure research to interpret remote sensing observations properly.

Keywords

Solar-induced chlorophyll fluorescence, gross primary production, vapor pressure deficit, photosynthetically active radiation, eddy covariance, radiative transfer model

Highlights

- The impact of aPAR and VPD on SIF was statistically decoupled and evaluated.
- GPP response to VPD was reproduced using proximal sensing of SIF and SCOPE model.
- aPAR and soil moisture are critical for evaluating SIF response to VPD.

1. Introduction

Solar-induced chlorophyll fluorescence (SIF) has been highlighted as a proxy for understanding plant physiology due to its strong relationship with gross primary production (GPP) across observational scales and direct ecophysiological connection with the light reactions in photosynthesis (Frankenberg et al., 2011; Guanter et al., 2014; Johnson & Berry, 2021; Kim et al., 2021; Porcar-Castell et al., 2014; Sun et al., 2017; Yang et al., 2015; Zhang et al., 2016a, 2018). SIF is often retrieved from satellite measurements (space-based), which have a coarse spatiotemporal scale. While space-based SIF retrieval is beneficial for understanding plant carbon dynamics at large scales (regional to global), its low temporal frequency in measurements (once per multiple days) may not be well-suited to studying physiological responses to fast-changing environmental drivers, limiting its utility to improve our understanding of ecophysiological response to climate change. For example, vapor pressure deficit (VPD, the difference between saturation and actual vapor pressure) is a function of air temperature and relative humidity and is thus highly variable diurnally. Moreover, VPD has received growing attention as an important environmental driver for its potential to affect plant biology (e.g., by inducing stomatal closure and limiting carbon uptake) and intensify hydrological cycles (e.g., more severe and frequent drought) due to the projected global warming in the future (Grossiord et al., 2020; López et al., 2021; McDowell et al., 2020, 2022; Novick et al., 2016a). For example, Wang et al. (2019) addressed the significant impact of increased VPD on the reduction of apparent SIF yield (defined as SIF divided by absorbed photosynthetically active radiation, aPAR) at a regional scale by leveraging the extreme drought and heatwave events in China. However, it is also essential to examine the SIF response over a range of VPD under moderate moisture conditions at a finer scale to elucidate the mechanisms of SIF response to changing VPD and its relationship with plant carbon uptake (e.g., GPP). Recent advances in automated tower-based SIF measurement techniques (Cogliati et al., 2015; Du et al., 2019; Grossmann et al., 2018; Gu et al., 2019; Guanter et al., 2013; Magney et al., 2019; Yang et al., 2015, 2018) have enabled high-frequency SIF measurement (< hourly interval) at a canopy scale.

However, it remains uncertain whether the effect of VPD on SIF can be confidently distinguished from SIF-aPAR at the canopy level. This is because SIF and aPAR are strongly correlated, and light intensity can indirectly influence VPD by increasing the temperature on sunny days since VPD is dependent on humidity and temperature (Chang et al., 2020; He et al., 2020; Miao et al., 2018). Paul-Limoges et al. (2018), for example, investigated the impact of VPD on SIF at a canopy scale using tower-based SIF measurement in a mixed forest and cropland, but without clear decoupling of VPD from the effect of aPAR. Moreover, while the importance of the definition of light absorption has been widely emphasized for remote-sensing-based photosynthesis observations (Ogutu & Dash, 2013; Yang et al., 2015; Zhang et al., 2020), previous studies often use photosynthetic photon flux density (PPFD) that may not accurately represent the actual amount of light absorbed by foliage or chlorophyll and used for photosynthesis; This is because PPFD measures the amount of PAR that actually arrives at the plant but does not distinguish PAR absorbed by non-photosynthetic components (e.g., stem, branch, senescent foliage) from photosynthetic components.

We evaluate the tower-based high-frequency SIF measurement (i.e., < hourly) as a tool to detect plant response to highly variable VPD by decoupling its impact from light availability. We used GPP estimated from eddy covariance measurement as a reference and compared it with the SIF measurement to test whether SIF and GPP have divergent or convergent responses to changing VPD. We also simulated SIF, aPAR, and quantum yields using the SCOPE model V1.73 (van der Tol et al., 2009) to compare with the SIF measurement. Our goal of the SCOPE simulation was to answer the following questions: 1) Does the pattern of the simulated SIF in response to VPD agree with the patterns of measurements? 2) If so, what is driving the observed response? If not, what are the major reasons for the discrepancy?

We further tested whether lower-frequency measurement of SIF (i.e., daily) is frequent enough to decouple the impact of VPD from aPAR by using the data collected around midday only. This test provides useful insight into the validity of low-frequency satellite measurements for studying the impact of highly variable VPD on SIF. Specifically, we defined the half-hourly measurement of SIF as ‘hourly scale’ data and the SIF measured between noon and 2 pm as ‘daily scale’ data and then compared these datasets.

2. Materials and Methods

2.1. Site Description

The study site (Virginia Forest Research Facility) is located in a temperate mixed forest, within the footprint of a flux tower in central Virginia, USA (37° 55'N 78° 16'W). Long-term mean annual temperature and precipitation (from 1981 to 2010) are 14.0°C and 1,210 mm (over 90% as rain), respectively. Canopy dominant tree species include white oak (*Quercus alba* L.), Virginia pine (*Pinus virginiana* Mill.), southern red oak (*Q. falcata* Michx.), red maple (*Acer rubrum* L.), and tulip poplar (*Liriodendron tulipifera* L.). The relative dominances (= basal area of a species / basal area of all trees × 100%) within a 500 m radius from the flux tower were 23.6%, 20.0%, 11.9%, 11.5%, and 10.3%, respectively (Chan, 2011). The range of diameter at breast height (DBH) was 2.5 to 81.0 cm, with tree sizes of second and third quartiles ranging from 4.0 to 15.1 cm. The study period was limited to the late growing season, from early July to mid-September in 2019, to minimize the effect of seasonality and the potential effect of sun-sensor-canopy geometrical variation.

2.2. SIF measured by Fluospec 2

SIF was measured using an automated system, Fluospec 2. A detailed description of the system is documented in Yang et al. (2018). The key component of the system is a high spectral resolution spectrometer (QEPro, OceanOptics Inc., Dunedin, FL, USA) with a spectral resolution of 0.14 nm and a spectral range of 729.7-784.1 nm. The main components of the system include a spectrometer, a computer for system operation (Raspberry Pi), and an optical shutter alternating the two optical cables that measure incoming solar radiation and upwelling radiation from canopies, respectively (Figure 1). For stability, the system is enclosed in a thermostatic box (25°C) inside an air-conditioned hut built to accommodate various research tools. The optical cables for radiance measurements are installed on the top platform of a flux tower.

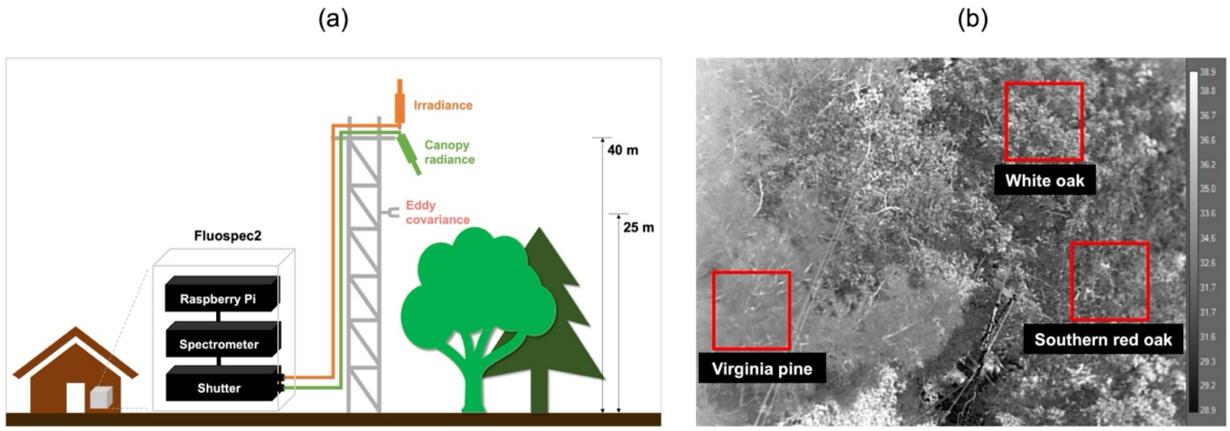

Figure 1. The design of instrument setup (Fluospec 2) at the study site (Virginia Forest Research Facility, a) and a sample thermal image taken at 13:00 EST on August 8, 2019 at the top platform of a flux tower near the SIF sensors (b). Fluospec 2 is composed of a SIF spectrometer, a computer for system operation (Raspberry Pi), and an optical shutter. The system is enclosed in a thermostatic box, with the temperature inside the enclosure set at 25°C, and resides inside a research hut. The ends of optical cables measuring irradiance and canopy radiance are installed on the top platform of a flux tower (40 m tall). Note that the field of view (FOV) of the optical fibers (25 degree) is smaller than the FOV of the thermal camera (45 degree). Thus, SIF is observed for a smaller area than appears in the thermal image in panel b.

We applied an O_2A-based spectral fitting method (SFM) that uses a reduced fitting window from 759.5 to 761.5 nm (Chang et al., 2020), which is known to improve O_2A retrieval accuracy compared to a conventional SFM method using a wider fitting window (759-767.76 nm). The SIF was recorded every 10 minutes and averaged every 30 minutes.

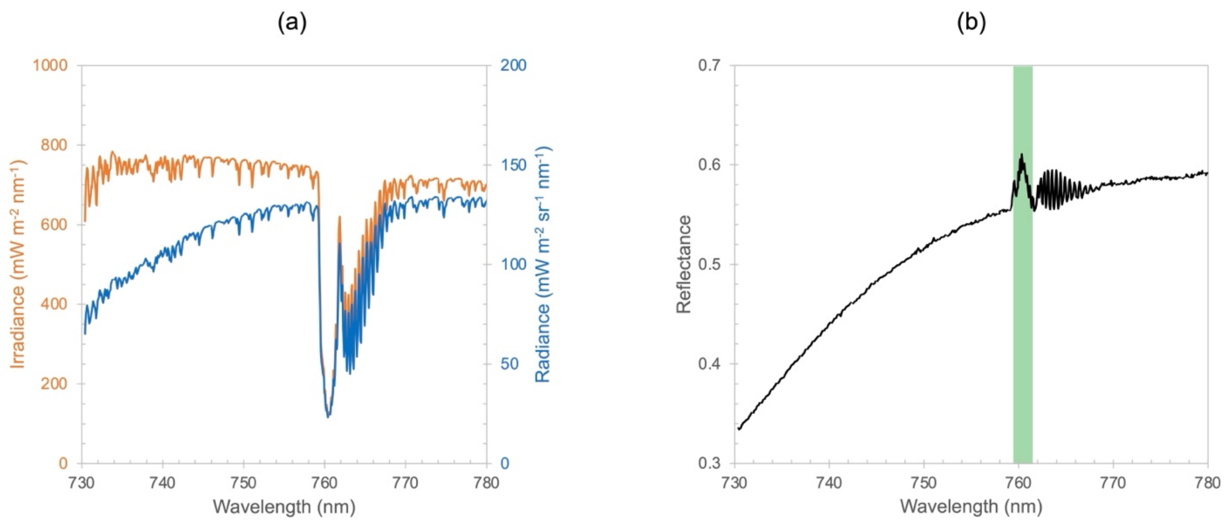

Figure 2. An example of data collected by Fluospec 2 at noon on June 14, 2019. Irradiance (orange in panel a) was collected by an upward-looking cosine corrector, and radiance (blue in panel a) was collected by an optical fiber pointing to the target tree canopy. Reflectance (b) was calculated by dividing radiance by irradiance and multiplying by π. The shaded area in green in panel b indicates the fitting window (759.5-761.5 nm) used for O_2A retrieval (Chang et al., 2020).

2.3. SIF simulated by SCOPE

We simulated SIF, aPAR, and quantum yields for the four pathways used by leaves during photosynthesis (i.e., quantum yields of photochemistry, Φ_P, fluorescence, Φ_F, non-photochemical quenching, Φ_N, and non-radiative decay, Φ_D) using the SCOPE model V1.73 (van der Tol et al., 2009). It is necessary to stress that the SCOPE simulations do not have to perfectly match the observations, and in fact, the mismatch between the observations and the model results is to be expected as several key parameters related to SIF (e.g., V_{cmax}: maximum carboxylation rate, FQE: fluorescence quantum yield efficiency at photosystem level) are prescribed. SCOPE model simulations were driven by meteorological data collected by the sensors installed at the study site, including PAR, longwave radiation, temperature, vapor and atmospheric pressure, and leaf area index from the Moderate Resolution Imaging spectroradiometer (MODIS, MCD15A2H Version 6; See Figure S1 in Supplementary Information for the variability of leaf area index). The model was modified to use the incident PAR measurements, instead of shortwave radiation, as input data for a more accurate aPAR simulation. The other inputs were set to default (See Table S1 in Supplementary Information for more details about the input data). We have compared two different fluorescence emission models (Moderate and Soil Moisture (SM) Stress models) incorporated in the SCOPE model, of which quantum yield fractions were set differently based on the experiments conducted under different soil moisture conditions (van der Tol et al., 2014). More specifically, van der Tol et al. (2014) demonstrated how fluorescence yield was influenced by non-photochemical quenching (Φ_N) using the results of previous studies that combined leaf gas exchange and pulse amplitude modulation (PAM) measurements. They compared multiple sets of experiments performed on different plants that were subject to different main environmental drivers, and developed two sets of parameters to model quantum yields for the SCOPE: one was based on the cotton dataset (Weis & Berry, 1987), concerned with light, CO_2, and temperature variations (without water stress; hereafter, 'Moderate mode'). Another set was based on C3 species treated with daily irrigation and then progressively decreasing soil moisture availability (Flexas et al., 1999; 2002); hereafter, 'Soil Moisture (SM) Stress mode' (See Discussions and Figure 10 for the comparison between two simulation modes). Therefore, the results from the two simulation modes would inform how the relationship between SIF and VPD depends on soil moisture conditions.

2.4. Eddy covariance and environmental drivers

CO_2, water, and energy fluxes and other environmental variables (e.g., air temperature, relative humidity, and VPD) were recorded by eddy flux tower using a sonic anemometer (CSAT3, Campbell Scientific, Logan, Utah), gas analyzer (LI-7500, Li-Cor, Lincoln, Nebraska), and temperature and humidity probe (HMP45, Vaisala, Helsinki, Finland) at a height of 25 m, several meters above the characteristic vegetation height. NEE partitioning into GPP and ecosystem respiration (R_{eco}) was done by using an R-based online eddy covariance processing tool, ReddyProc (Wutzler et al., 2018) and choosing the daytime partitioning algorithm. Compared to another partitioning option available in the ReddyProc (i.e., nighttime partitioning algorithm), the daytime partitioning algorithm accounts for the temperature sensitivity of R_{eco} and the effect of VPD on plant light response curve to enhance the reliability of R_{eco} estimates (Lasslop et al., 2010). Only GPP greater than 5 μmol m^{-2} s^{-1} was used for the analysis to avoid the poorly defined relationship between GPP and aPAR under the conditions of low GPP. The temporal resolution of GPP and ancillary data was 30 minutes.

2.5. aPAR estimation

Careful selection of aPAR definition is important because aPAR is often estimated in different ways based on the different assumptions of light absorption (Porcar-Castell et al., 2021). For example, an assumption of a whole canopy as a light absorbent does not discern differences in light absorption between photosynthetic (i.e., functional leaves) and non-photosynthetic (i.e., stem, branches, and senescent leaves) components, in contrast to the assumption of photosynthetically functional leaves as the only light absorbent. Furthermore, the close relationship between SIF and aPAR may have a significant influence when evaluating the impact of other environmental factors on SIF. We have compared four different approaches to estimate aPAR: PAR absorbed by the entire canopy, which is estimated by stand-scale measurement ($aPAR_m$), PAR absorbed by chlorophyll ($aPAR_{chl}$), reflected radiance in the far-red spectrum at 755 nm measured by Fluospec 2 (Rad755), and aPAR estimated by SCOPE simulation ($aPAR_{sc}$).

The $aPAR_m$ was estimated by simultaneous in-situ measurements at different positions using quantum sensors (PQS-1, Kipp & Zonen B.V., Delft, Netherlands) as follows:

$$aPAR_m = PAR_{above} - PAR_{under} - PAR_{refl} \qquad (1)$$

where PAR_{above} is PAR measured above canopies, PAR_{under} is an average of PAR measured at three different positions under canopies, and PAR_{refl} is canopy-reflected PAR. The PAR components were measured every minute and averaged every 30 minutes to match its temporal resolution with GPP and SIF. The $aPAR_m$ represents a conventional method to estimate site-level aPAR.

The approach to estimating $aPAR_{chl}$ was suggested by Ogutu and Dash (2013). According to their definition, $aPAR_{chl}$ is PAR absorbed by photosynthetic components of canopies only (i.e., excluding PAR absorbed by branches, stem, and senescent foliage) and utilized for photosynthesis. Therefore, unlike $aPAR_m$, $aPAR_{chl}$ represents aPAR at the level of organelles. The $aPAR_{chl}$ can be estimated by using eddy covariance data from the following equation:

$$aPAR_{chl} = \text{incident PAR} \times faPAR_{chl} = (\text{NEE} - R_{eco}) / \alpha_a \qquad (2)$$

where $faPAR_{chl}$ is the fraction of aPAR absorbed by photosynthetic elements in the canopy, NEE is net ecosystem exchange (μmol m^{-2} s^{-1}), α_a is actual quantum yield (the number of moles of CO_2 fixed per mole of PAR absorbed by photosynthetic elements in the canopy: mol mol^{-1}), which is a function of maximum intrinsic quantum yield (0.08 mol mol^{-1} for C3 plants) (Collatz et al., 1991; Hanan et al., 2002), air temperature, and VPD, and R_{eco} is ecosystem respiration (μmol m^{-2} s^{-1}) (Refer to Ogutu & Dash (2013) for more details about the derivation). While actual quantum yield is a function of VPD, we applied a constant VPD representing VPD in clear midday during the study period from July to September (2 kPa) to avoid the potential perplexing influence of both VPD and $aPAR_{chl}$ on GPP and SIF (see Figure S2 in Supplementary Information for the comparison between $aPAR_{chl}$ estimated using constant VPD and variable VPD).

The radiance in the far-red spectrum reflected by canopies (Rad755) is often used to derive relative SIF (=SIF/Rad755). Relative SIF is the normalized SIF to correct the effect of heterogeneous vegetation structure (Magney et al., 2019; Parazoo et al., 2020) and is comparable to SIF yield (=SIF/aPAR). In principle, relative SIF is comparable to the near-infrared radiance of vegetation (NIRvR) when Normalized Difference Vegetation Index (NDVI) is stable, as NIRvR is approximately NDVI multiplied by observed NIR radiance (NIRrad), where NIRrad is linearly related with aPAR (Zeng et al., 2019). Therefore, although Rad755 may not represent aPAR in principle, we tested the possibility of Rad755 as a proxy of aPAR to address the impact of VPD on SIF. In addition, one benefit of using relative SIF is that the radiance at 755 nm was observed from the same footprint as the SIF measurements.

Lastly, PAR absorbed by chlorophyll *a* and *b* simulated by SCOPE ($aPAR_{sc}$) was used against simulated SIF. The simulation of $aPAR_{sc}$ is based on in-situ measurement of incident PAR, radiative transfer, and chlorophyll absorption spectrum.

Table 1. Definitions of aPAR metrics used in this study.

aPAR metrics	Description
$aPAR_m$	aPAR estimated by simultaneous in-situ measurements of PAR at different positions using quantum sensors. $aPAR_m = PAR_{above} - PAR_{under} - PAR_{refl}$ • PAR_{above}: PAR measured above canopies • PAR_{under}: average of PAR measured at three different positions under canopies • PAR_{refl}: canopy-reflected PAR
$aPAR_{chl}$	PAR absorbed by photosynthetic components of canopies only (i.e., excluding PAR absorbed by branches, stem, and senescent foliage) and utilized for photosynthesis (Ogutu & Dash, 2013). $aPAR_{chl}$ = incident PAR × $faPAR_{chl} = (NEE - R_{eco}) / \alpha_a$ • $faPAR_{chl}$: the fraction of aPAR absorbed by photosynthetic elements in the canopy • NEE: net ecosystem exchange (μmol m^{-2} s^{-1}) • α_a: actual quantum yield (the number of moles of CO_2 fixed per mole of PAR absorbed by photosynthetic elements in the canopy: mol mol^{-1}) • R_{eco}: ecosystem respiration (μmol m^{-2} s^{-1})
Rad755	The radiance in the far-red spectrum reflected by canopies, which is often used to derive relative SIF (= SIF/Rad755).
$aPAR_{sc}$	PAR absorbed by chlorophyll *a* and *b* simulated by SCOPE.

2.6. Data analyses

Our primary interest in this study is to understand the impact of VPD on SIF. However, SIF is known to have a strong linear relationship with aPAR. Therefore, we must confidently decouple the impact of VPD from the relationship between SIF and aPAR. We used the Johnson-Neyman technique (Bauer & Curran, 2005; Johnson & Fay, 1950) to evaluate the interaction between aPAR and VPD and its influence on SIF or GPP. We then compared linear regressions of SIF (or GPP) and aPAR at different levels of VPD by performing Simple slopes analysis (Aiken & West, 1991). While the one-way analysis of covariance (ANCOVA) is often performed for this type of situation, our cases violate the assumption of homogeneity of the regression slopes; in other words, we have non-parallel regression slopes of SIF-aPAR across different levels of VPD. The Johnson-Neyman technique addresses this issue by identifying the interval of aPAR in which the influence of VPD on SIF-aPAR regression (∂SIF/∂VPD) is significant or insignificant (at a level of 0.05 in our case).

In the results, we illustrate 1) the range of aPAR values where VPD has a significant influence on SIF-aPAR regression and 2) how SIF-aPAR regressions differ at three separate VPD levels (at mean VPD, mean VPD plus 1.5 times standard deviation, and mean VPD minus 1.5 times standard deviation). We hypothesized that the response of SIF is mainly attributable to the variability of Φ_F, given negligible variations in the canopy structure and thus f_{esc} during the growing season when the canopy is closed (He et al., 2020). Based on our SCOPE simulation, only up to 3% of the variability in f_{esc} was found throughout the study period.

In order to meet the assumption of linearity between the dependent variable (SIF) and the moderator (aPAR), both variables were log-transformed using natural log, such that the non-linear power function for the SIF-aPAR relationship (i.e., SIF = a·aPAR^b) was transformed into the linear function between ln(SIF) and ln(aPAR) (i.e., ln(SIF) = ln a + b·ln(aPAR), where b is the slope and ln a is the intercept in the transformed relationships, Figure 3). We performed the same analysis for GPP by log-transforming both GPP and aPAR (i.e., GPP = a·aPAR^b) as a reference.

Lastly, we further tested the response of SIF using the data collected during the midday only (12 - 2 pm), which represents low-frequency observations such as satellite or airborne measurements, to find out whether we could find a similar response compared to full-day SIF response and/or GPP response.

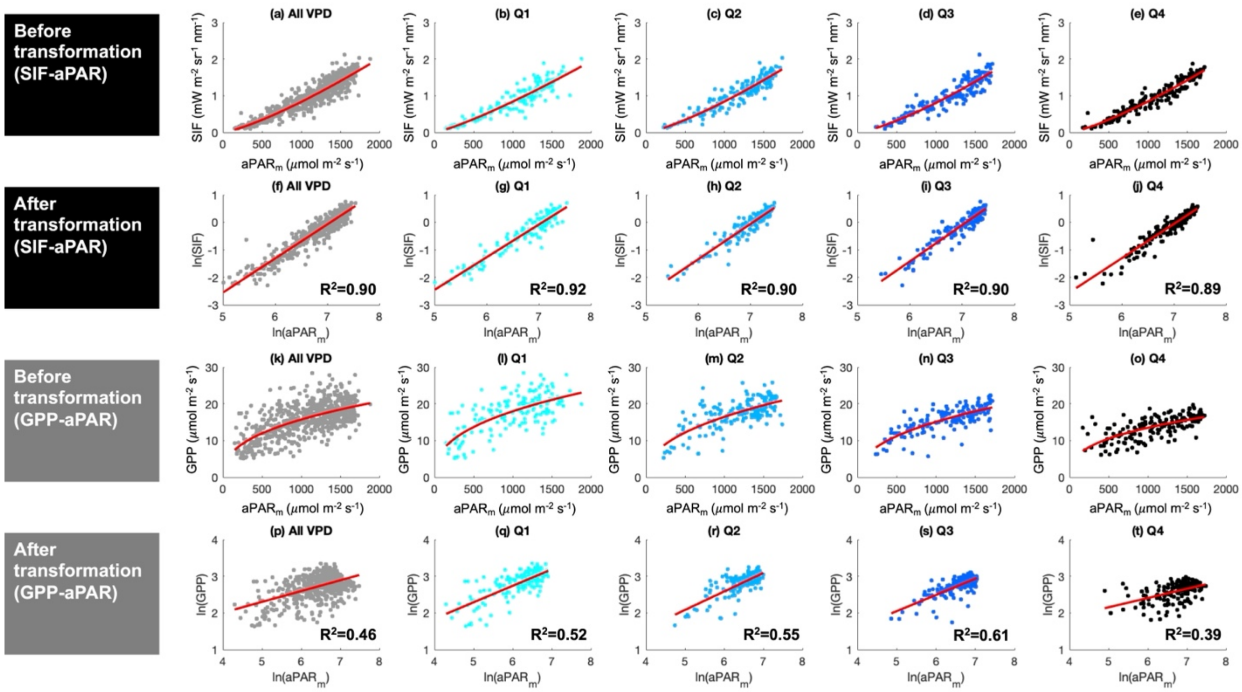

Figure 3. Example of data transformation of SIF, GPP, and aPAR for different levels of VPD (grouped based on the quartiles of the VPD distribution, Q1: 0.0 - 1.3 kPa, Q2: 1.3 - 1.9 kPa, Q3: 1.9 - 2.5 kPa, and Q4: 2.5 - 3.7 kPa). The non-linear power functions for the SIF-aPAR (SIF = $a \cdot \text{aPAR}^b$) and GPP-aPAR relationships (GPP = $a \cdot \text{aPAR}^b$) were transformed by applying natural log to both sides of the equation (e.g., $\ln(\text{SIF}) = \ln a + b \cdot \ln(\text{aPAR})$, where b is the slope, and $\ln a$ is the intercept in the transformed relationships.)

3. Results

3.1. Diurnal and seasonal patterns of GPP and SIF

As has been widely observed in many studies, GPP, measured SIF (SIF_{FS2}), and simulated SIF (SIF_{SC}) all have unimodal diurnal patterns that increase in the morning, peak around noon, and gradually decrease in the afternoon (Figure 4). As expected, diurnal patterns of GPP and SIF correspond well to the pattern of incident PAR (iPAR). Meanwhile, VPD and T_a show delayed peaks around 3 pm compared to GPP, SIF, and iPAR. Compared to the diurnal patterns of SIF, the decreasing rate of GPP in the afternoon is slower. For instance, SIF started with a low value at 6 am and returned to a similar level at or before 6 pm. On the other hand, GPP did not return to a similar level observed at 6 am by 6 pm.

The seasonal trends of GPP and SIF_{FS2} were similar to each other (Figure 4). Specifically, both GPP and SIF_{FS2} were highest during the early growing season (May) and gradually decreased for the rest of the season. However, the seasonal pattern of SIF_{SC} was different compared to the GPP or SIF_{FS2}. The SIF_{SC} gradually increased during the early growing season, remained high during the summer (June to August), and decreased afterward. This pattern coincided with the seasonal pattern of iPAR.

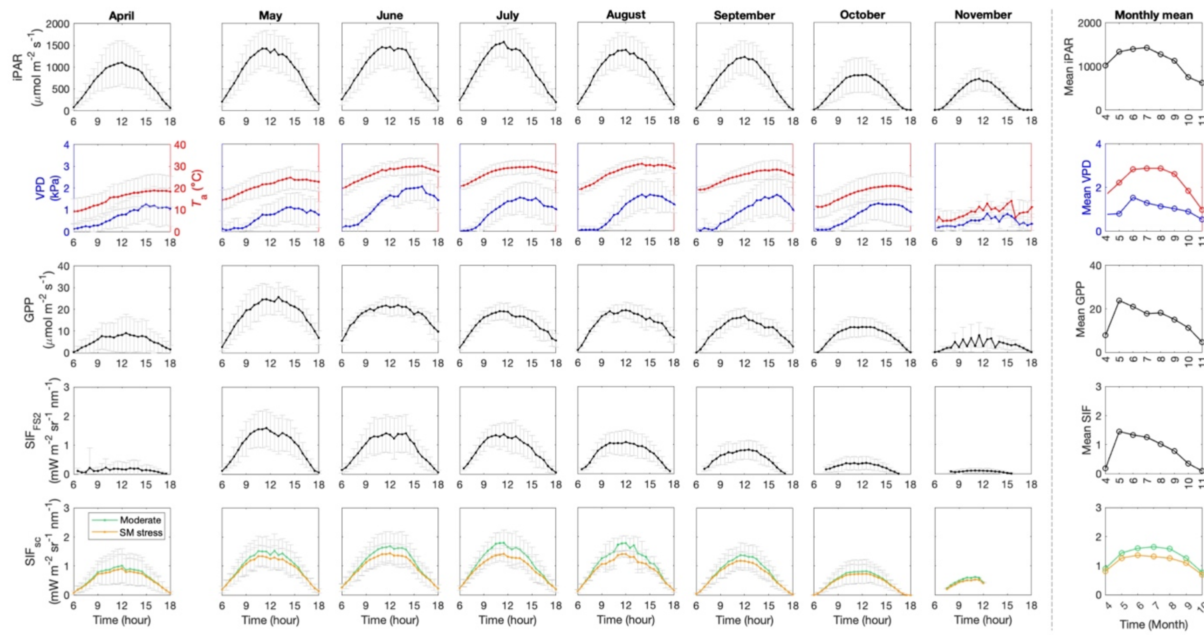

Figure 4. Monthly mean diurnal patterns of GPP estimated from the eddy covariance method, SIF measured by Fluospec 2 (SIF_{FS2}), SIF simulated by SCOPE (SIF_{SC}), and environmental variables including incident PAR (iPAR), vapor pressure deficit (VPD), and air temperature (T_a), and their monthly mean between 10 am to 2 pm. Error bars represent standard deviations.

3.2. Comparison between aPAR metrics

All aPAR metrics were linearly related to the iPAR but with different slopes and variances (Figure 5). Among the metrics, $aPAR_m$ had the least deviation from iPAR (slope = 0.94) with a very high R^2 of the regression (= 0.995). The aPAR simulated by SCOPE ($aPAR_{sc}$) was also proportional to the iPAR and had a very high R^2 of the regression (= 0.999) but with appreciable deviation (slope = 0.72) from iPAR. On the other hand, $aPAR_{chl}$ deviated from iPAR appreciably (slope = 0.66) with lower R^2 of the regression (= 0.755) than $aPAR_m$ and $aPAR_{SC}$. This reflects a characteristic of $aPAR_{chl}$, which assumes variable aPAR utilization for photosynthesis depending on environmental conditions (Ogutu & Dash, 2013) and thus requires additional environmental variables, other than iPAR, to better predict its variation. Similarly, Rad755 also had a lower R^2 of the regression (= 0.849) than $aPAR_m$ or $aPAR_{sc}$, implying its susceptibility to environmental variables other than light conditions.

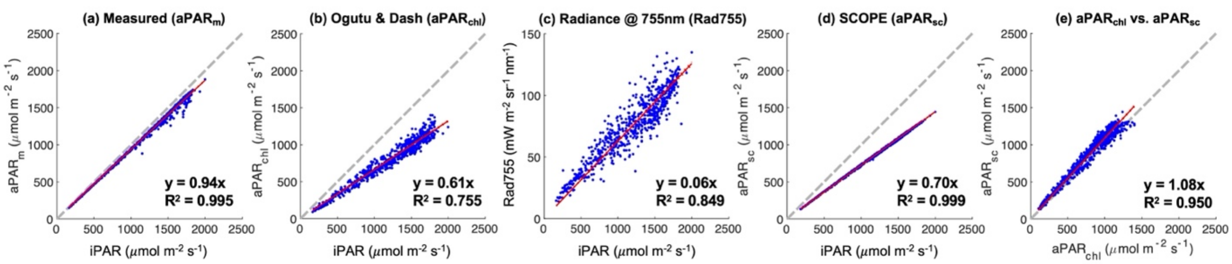

Figure 5. Relationships between incident PAR (iPAR) and different absorbed PAR (aPAR) metrics. Gray dashed lines indicate a 1:1 line. Red solid lines indicate linear regression fit.

3.3. Response of GPP and SIF to changing aPAR and VPD

According to the Johnson-Neyman technique results, the influence of VPD on the GPP-aPAR regression was significant regardless of the aPAR metrics during most of the daylight conditions (Figure 6a-6d). Specifically, VPD had a significant impact when log-transformed $aPAR_m$, $aPAR_{chl}$, Rad755, and $aPAR_{sc}$ were greater than 5.42, 4.93, 2.88, and 5.29, respectively. These values correspond to 225.9, 138.4, 17.8, and 198.3 μmol m^{-2} s^{-1}, respectively, before transformation (see Figure 4 for the daily variation of iPAR over the growing season and Figure 5 for the relationships between iPAR and aPAR metrics). In all cases, GPP decreased with rising VPD (Figure 6i-6l). The impact of VPD on GPP was more evident under higher aPAR.

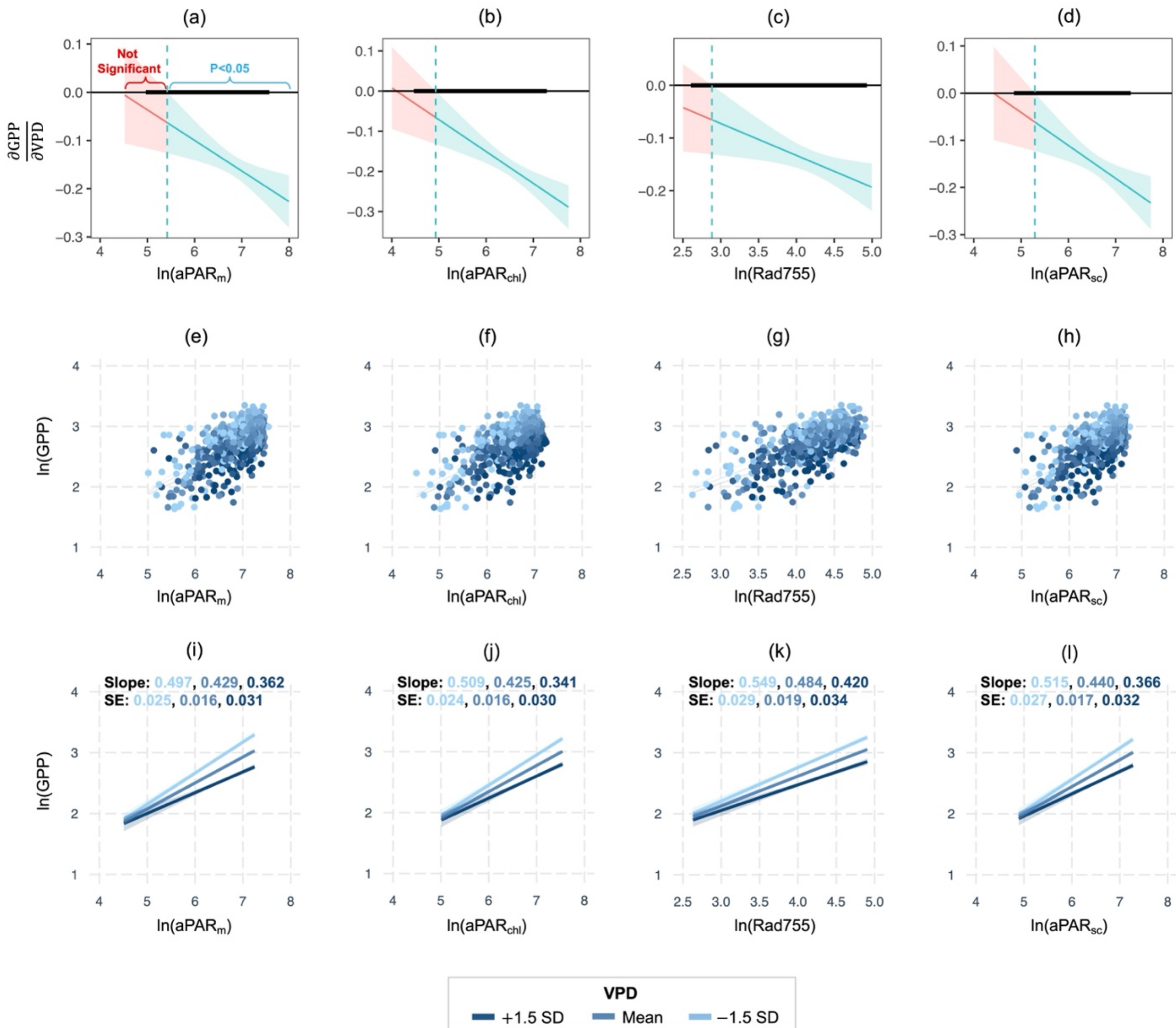

Figure 6. Effect of VPD on GPP-aPAR relationship at hourly scale. The top row (a-d) shows the results of Johnson-Neyman analysis, identifying the range of aPAR metrics where the influence of VPD on GPP-aPAR regression is significant (P < 0.05, shaded in green). The thicker horizontal lines at 0 in Johnson-Neyman plots indicate the observed range of aPAR metrics. The middle row (e-h) shows scatter plots of log-transformed and GPP and aPAR metrics. The bottom row (i-l) shows the results of Simple slopes analysis, illustrating GPP-aPAR regressions held at three VPD levels: mean VPD, mean VPD plus 1.5 times standard deviation, and mean VPD minus 1.5 times standard deviation. Note that confidence intervals are illustrated in gray around

the fitted lines (i-l) but are barely visible because they are very narrow, especially under high aPAR. Slope and standard error (SE) values are presented (i-l), and the text colors match the colors of the fitted lines.

Unlike GPP, we found inconsistent results depending on the aPAR metrics or SIF estimation method (Figure 7). The influence of VPD on the SIF was significant for the wide range of aPAR values when $aPAR_{chl}$ was used (Figure 7b) or SIF and aPAR were simulated with SCOPE (Figure 7d & 7e). On the other hand, the influence of VPD was insignificant over the entire range of observed $aPAR_{m}$ (Figure 7a) and over more than half of the observed range of Rad755 (Figure 7c).

SIF decreased with rising VPD – the pattern consistent with GPP – only when $aPAR_{chl}$ was used (Figure 7l) or when SIF and aPAR were simulated using the SM Stress mode (Figure 7o). In the case where SIF and aPAR were simulated using the Moderate mode (Figure 7n), VPD influenced SIF negatively when $\ln(aPAR_{sc})$ was less than 6.50 (i.e., $aPAR_{sc}$ = 665 µmol m^{-2} s^{-1}) but positively when $\ln(aPAR_{sc})$ was greater than 6.78 (i.e., $aPAR_{sc}$ = 880 µmol m^{-2} s^{-1}). When Rad755 was used, VPD had a positive effect on hourly SIF under high Rad755 conditions, which was the opposite of VPD's effect on GPP (Figure 7m).

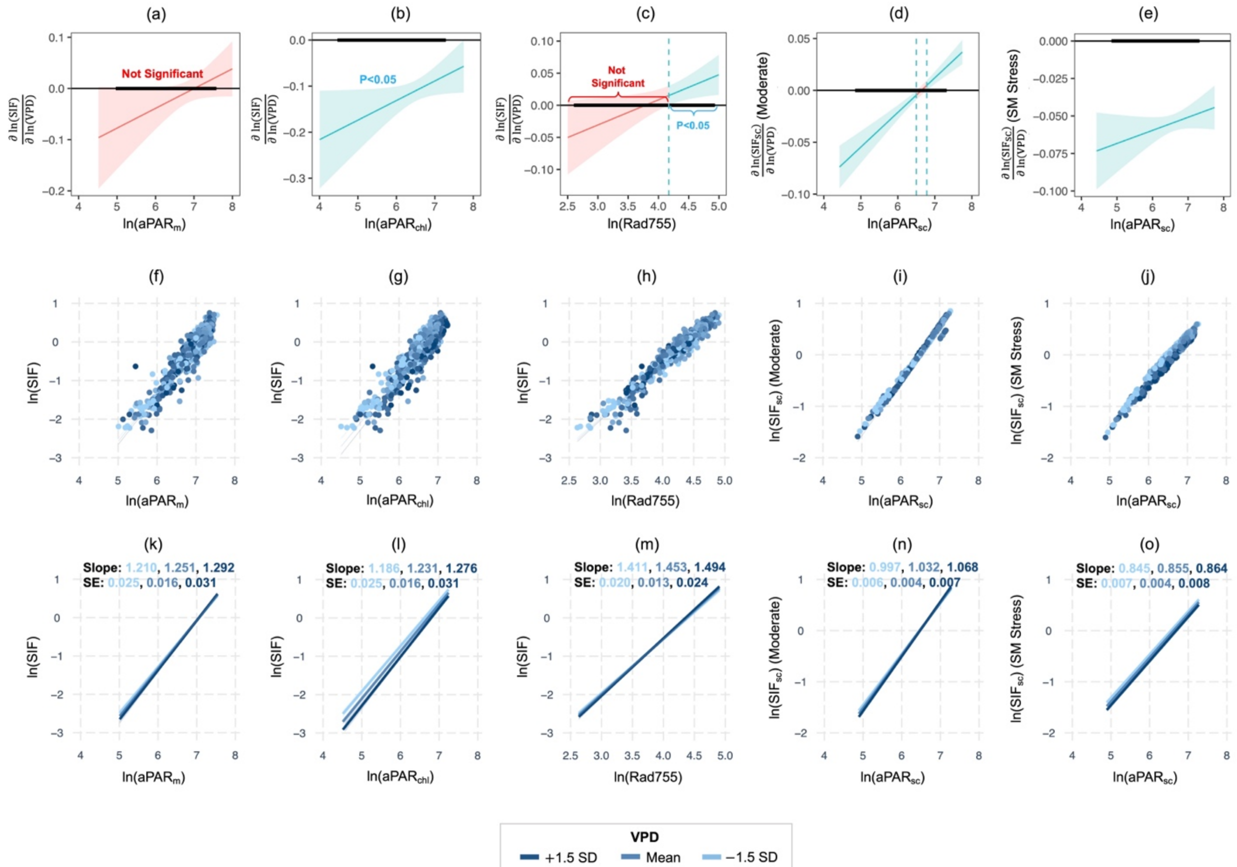

Figure 7. Effect of VPD on SIF-aPAR relationship at hourly scale. The top row (a-e) shows the results of Johnson-Neyman analysis, identifying the range of aPAR metrics where the influence of VPD on SIF-aPAR regression is significant ($P < 0.05$, shaded in green). The thicker horizontal lines at 0 in Johnson-Neyman plots indicate the observed range of aPAR metrics. The middle row (f-j) shows scatter plots of log-transformed and SIF and aPAR metrics. The bottom row (k-o) shows the results of Simple slopes analysis, illustrating SIF-aPAR regressions held at three VPD levels: mean VPD, mean VPD plus 1.5 times standard deviation, and mean VPD minus 1.5 times standard deviation. Note that confidence intervals are illustrated in gray around the fitted lines (k-o) but are barely visible because they are very narrow, especially under high aPAR. Slope and standard error (SE) values are presented (k-o), and the text colors match the colors of the fitted lines.

The daily scale relationships between log-transformed SIF and aPAR (Figure 8) were similar to the hourly scale relationship (Figure 7). VPD had a negative influence on daily SIF when $aPAR_{chl}$ was used (Figure 8l) or when SIF and aPAR were simulated with SCOPE using the SM Stress mode (Figure 8o). Although the range of aPAR where VPD significantly influences daily-scale SIF was smaller (Figure 8b & 8e) compared to the hourly-scale results (Figure 7b & 7e), the aPAR conditions still represent a wide range of daylight conditions enabling active photosynthesis. For example, VPD had a negative effect on SIF when $\ln(aPAR_{chl})$ was higher than 5.50 (i.e., $aPAR_{chl} > 245$ µmol m^{-2} s^{-1}, Figure 8l) or when SIF and aPAR were simulated using the SM Stress mode and $\ln(aPAR_{sc})$ was higher than 5.95 (i.e., $aPAR_{sc} > 384$ µmol m^{-2} s^{-1}, Figure 8o). When using $aPAR_m$, however, the effect of VPD on SIF was significant when $\ln(aPAR_m)$ was between 5.94 and 6.64 (i.e., $aPAR_m$ is between 380 and 765 µmol m^{-2} s^{-1}, Figure 8a), which represents relatively low daylight conditions. When Rad755 was used, VPD influenced daily SIF positively under low Rad755 conditions, which was opposite to the impact of VPD on GPP (Figure 8m).

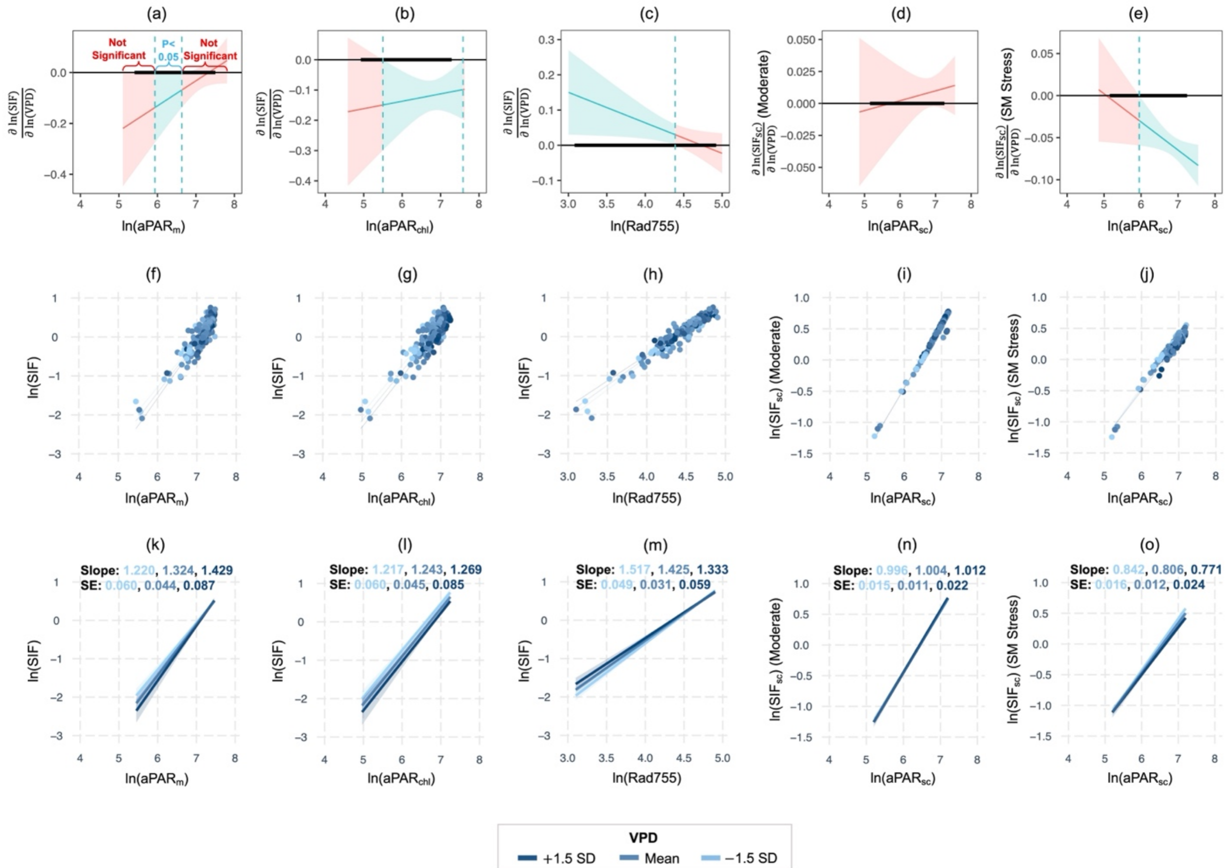

Figure 8. Effect of VPD on SIF-aPAR relationship at daily scale. The top row (a-e) shows the results of Johnson-Neyman analysis, identifying the range of aPAR metrics where the influence of VPD on SIF-aPAR regression is significant ($P < 0.05$, shaded in green). The thicker horizontal lines at 0 in Johnson-Neyman plots indicate the observed range of aPAR metrics. The middle row (f-j) shows scatter plots of log-transformed and SIF and aPAR metrics. The bottom row (k-o) shows the results of the Simple slopes analysis, illustrating SIF-aPAR regressions held at three VPD levels: mean VPD, mean VPD plus 1.5 times standard deviation, and mean VPD minus 1.5 times standard deviation. Note that confidence intervals are illustrated in gray around the fitted lines (k-o) but are barely visible because they are very narrow, especially under high aPAR. Slope and standard error (SE) values are presented (k-o), and the text colors match the colors of the fitted lines.

The relationship between GPP and SIF was non-linear at both hourly and daily scales due to the steeper slope at low GPP and SIF (Figure 9). However, the relationship was strongly linear for most SIF and GPP ranges once SIF or GPP exceeded a certain level. Although daily scale observations had a lower coefficient of determination than hourly scale observations, we found similar variability in the GPP-SIF relationship with changing VPD at both temporal scales. When the GPP-SIF relationship was fitted using a power function (i.e., GPP = $k \times$ SIF^a) at either scale, the coefficient k decreased with rising VPD (Figures 9b & 9e). However, the exponent a did not vary significantly (Figures 9c & 9f).

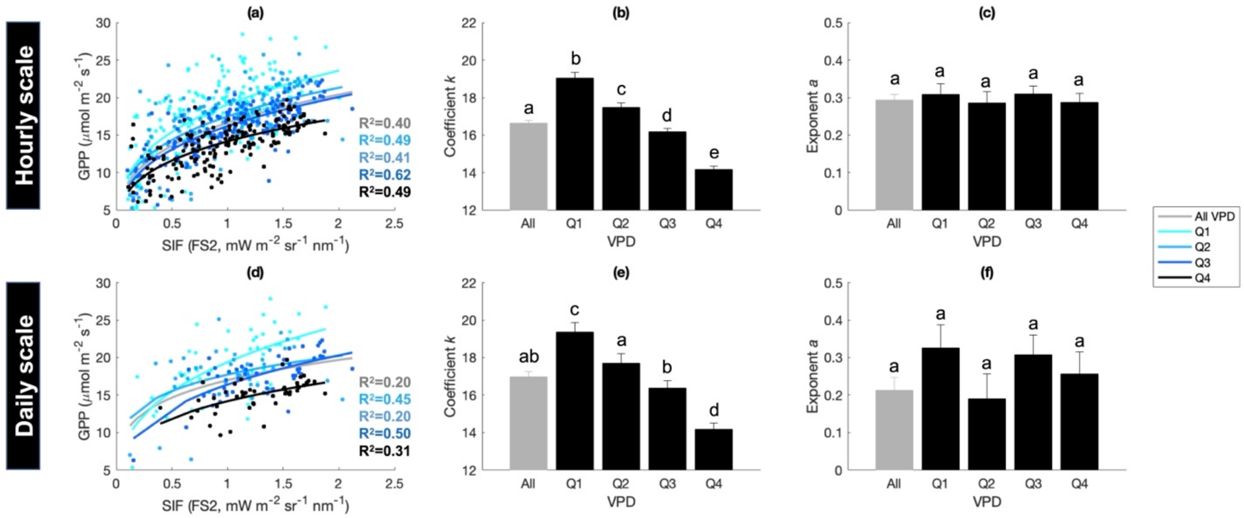

Figure 9. Non-linear relationships between GPP and SIF measured by Fluospec 2 at different levels of VPD (grouped based on the quartiles of the VPD distribution, Q1: 0.0 - 1.3 kPa, Q2: 1.3 - 1.9 kPa, Q3: 1.9 - 2.5 kPa, and Q4: 2.5 - 3.7 kPa) at hourly (a, b, c) and daily scales (d, e, f). The GPP-SIF relationships were fitted using a power function (i.e., GPP = $k \times$ SIF^a). Error bars

represent standard errors of means (95% confidence). Coefficient *k* (b & e) or exponent *a* (c & f) marked with different letters are significantly different ($p < 0.05$).

4. Discussions

We investigated SIF variations in response to changing VPD at a canopy scale using tower-based SIF measurements in a temperate forest. Specifically, we tested if using different definitions for aPAR and temporal scales (i.e., hourly vs. daily) would influence SIF response to changing VPD.

SIF is considered a remotely sensed proxy for GPP because of its good relationship with GPP across various observational scales. However, while GPP represents the carbon assimilated as a result of photosynthesis, SIF is the energy re-emitted after light absorption by leaf chlorophyll molecules (a different pathway than the pathway routed for photosynthesis). Despite the close link of SIF to plant photochemistry, SIF is not equivalent to photosynthetic carbon uptake and GPP. Therefore, the interaction of SIF with environmental variables may not necessarily be the same as GPP.

We found a SIF response to VPD that corresponded to the GPP response to VPD when PAR absorbed by chlorophyll ($aPAR_{chl}$) was used or when SIF and aPAR were simulated by SCOPE model that was parameterized to account for the effects of soil moisture stress (i.e., SM Stress mode). Our findings suggest that tower-based SIF measurement has the potential to address the impact of water stress on ecosystem function.

The definition of aPAR was critical for SIF to emulate GPP response to VPD. SIF was negatively related to VPD only when $aPAR_{chl}$ was used or SIF and aPAR were simulated by SCOPE on the SM Stress mode. This emphasizes the importance of carefully defining and evaluating light conditions, or more precisely, light availability to vegetation, especially when addressing the impact of environmental drivers other than light conditions on SIF.

Among the aPAR metrics, $aPAR_{chl}$ was defined as the PAR absorbed by the photosynthetic component of the canopy (i.e., green foliage). In other words, $aPAR_{chl}$ represents aPAR at the foliage or organelle (chlorophyll) level, which agrees with the SIF emission level (Zhang et al., 2016b). Therefore, $aPAR_{chl}$ is expected to account for the effects of environmental drivers on photosynthesis (e.g., air temperature, moisture condition, and nutrient availability), while the other aPAR metrics don't. Indeed, in the algorithm of $aPAR_{chl}$ estimation, the process of estimating actual quantum yield (i.e., the number of moles of CO_2 fixed per mole of PAR absorbed by photosynthetic elements in the canopy) is an empirical function of air temperature. As a result, the relationship between $aPAR_{chl}$ and iPAR has a low R^2 when compared to the other aPAR metrics (Figure 5). Although the rigorous verification of $aPAR_{chl}$ is difficult, the similarity between $aPAR_{chl}$ and aPAR simulated by SCOPE supported the legitimacy of $aPAR_{chl}$ (Figure 5e). Furthermore, we found a negative effect of VPD on SIF when $aPAR_{chl}$ was used (Figures 7 & 8), which is consistent with the effect on GPP (Figure 6). It is important to note that we applied a constant VPD to estimate the actual quantum yield for $aPAR_{chl}$, which had a lower variance than the $aPAR_{chl}$ estimated using a variable VPD (See Figure S2 in Supplementary Information). In our preliminary analysis, we found similar trends in SIF in response to changing VPD whether constant or variable VPD was used for $aPAR_{chl}$ estimation: the only difference was that SIF variability in response to changing VPD was greater when $aPAR_{chl}$ was estimated by using variable VPD rather than constant VPD (See Figure S3 for the hourly-scale result and Figure S4 for the daily-scale result in Supplementary Information). Overall, we confirm that $aPAR_{chl}$ is likely to reflect the actual amount and variability of PAR absorbed by the foliage and used for photosynthesis, and that the impact of $aPAR_{chl}$ on SIF demonstrated in our study (i.e., $aPAR_{chl}$ estimated by using a constant VPD) is likely to be conservative.

Meanwhile, $aPAR_m$ is the PAR absorbed by any components of the canopy, including non-photosynthetic components (e.g., branches, stems, and senescent foliage) that are irrelevant to SIF emission. Because it accounts for insensitive non-photosynthetic components, using $aPAR_m$ my result in a less sensitive photosynthetic response than expected. For example, a very small variance was found in the relationship between $aPAR_m$ and iPAR (Figure 5a), implying that environmental drivers other than iPAR had a negligible effect on the $aPAR_m$. Therefore, the disparity in scope of measurement between SIF and $aPAR_m$ (i.e., photosynthetic component only vs. photosynthetic and non-photosynthetic components) should have contributed to the ambiguous effect of VPD on the SIF-$aPAR_m$ relationship (Figure 7).

In contrast to the GPP-VPD relationship, we found a positive effect of VPD on SIF when Rad755 was used as a proxy of aPAR although there is no theoretical basis for describing the opposite pattern. Therefore, while Rad755 may be useful as a proxy of aPAR to approximate GPP and SIF due to its strong relationship with iPAR, it is less useful when the effect of environmental drivers other than light conditions must be considered.

While we suggest using an aPAR definition that can be estimated from eddy covariance data (i.e., $aPAR_{chl}$) among the tested metrics, it may be preferable to use aPAR metrics that can be estimated more easily for larger-scale observations. Zhang et al. (2020), for example, compared the fraction of PAR absorbed by chlorophyll (faPAR) obtained from six different satellite products. Further research into how different definitions of the faPAR affect SIF and its response to changing environmental drivers is needed to improve the utility of SIF as a proxy for GPP because faPAR is heavily influenced by the canopy structure, including leaf-angle distributions (Stovall et al., 2021; Yang et al., 2023). Future research into leaf-angle distribution and its temporal variations, for instance, using recent terrestrial light detection and ranging (lidar) techniques, would help improve our understanding of the impact of canopy structure on faPAR and SIF.

We used SCOPE to simulate SIF with two different modes of fluorescence emission, Moderate and SM Stress, to compare with measured SIF and infer the mechanism of SIF response to VPD and soil moisture. The expected negative effect of VPD on SIF emerged when the SM Stress mode was used. When the response of quantum yields to aPAR was compared between the simulation modes, the response of fluorescence yield (Φ_F) was found to be the most different (Figure 10; also refer to van der Tol et al. (2014) and Verrelst et al. (2015)). Specifically, in the case of the Moderate mode, Φ_F decreased rapidly with increasing aPAR under low aPAR, but there was little change under moderate to high aPAR (Figure 10b). In the SM Stress mode, on the other hand, a negative relationship between Φ_F and aPAR was found across the entire range of aPAR (Figure 10f). The patterns of Φ_F found in both simulation modes were consistent with the descriptions in van der Tol et al. (2014), which suggested decreasing Φ_F as an indication of water stress. Moreover, with the SM Stress mode, we found a reduction of Φ_F across the entire range of aPAR with rising VPD (Figure 10). Considering the variability of Φ_F in the SCOPE is mainly driven by aPAR and carboxylation capacity (van der Tol et al., 2014), the results of SIF simulation should be mainly reflective of the negative impact of VPD, temperature (due to VPD being a function of temperature), and/or soil moisture, on the non-stomatal processes.

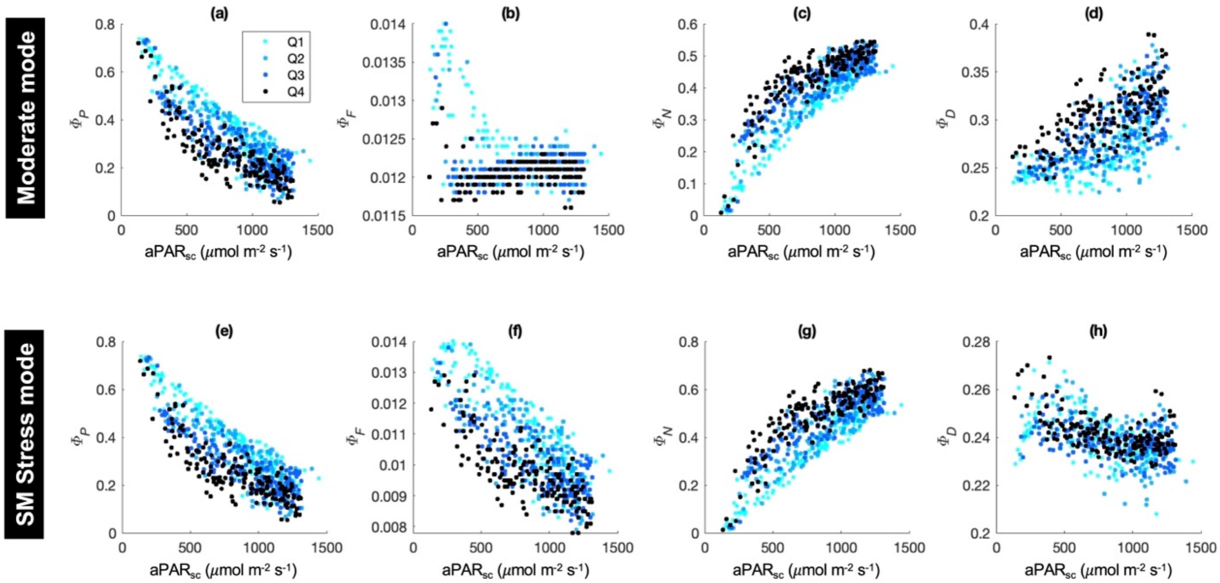

Figure 10. Variations of quantum yields (Φ_P: photochemistry, Φ_F: fluorescence, Φ_N: non-photochemical quenching, Φ_D: non-radiative decay) with changing aPAR simulated by SCOPE using two different modes (i.e., Moderate and SM Stress modes) across different VPD levels (grouped based on the quartiles of the VPD distribution, Q1: 0.0 - 1.3 kPa, Q2: 1.3 - 1.9 kPa, Q3: 1.9 - 2.5 kPa, and Q4: 2.5 - 3.7 kPa).

The simulation results of quantum yields (Figure 10), as well as interactions between SIF_{sc}, $aPAR_{sc}$, and VPD (Figures 6 & 8), indicate that the SIF-VPD relationship is dependent on soil moisture conditions. This implies that the negative effect of VPD on SIF observed when using $aPAR_{chl}$ (Figure 6 & 8) may be driven by both VPD and soil moisture conditions. This is consistent with previous research (Liu et al., 2020), which investigated the relative effect of VPD and soil moisture on satellite-based SIF. Our study site is a mesic temperate forest with plenty of rainfall (long-term mean annual precipitation = 1,210 mm), a moderate level of soil moisture (i.e., volumetric water content over the study period (mean $\pm$ standard deviation) = 0.33 $\pm$ 0.05 m^3 m^{-3}), and a low correlation between soil moisture and VPD (0.17 at the hourly scale and 0.12

at the daily scale). We note that the impact of soil moisture on SIF was only implied by the SCOPE simulation and was not evaluated by in-situ data in our study, due to the limited amount of data to decouple the effect of soil moisture, VPD and aPAR. Long-term, high-frequency data collection will aid in decoupling the impact of multiple environmental drivers on SIF, which is a significant advantage of tower-based SIF measurements over other methods.

Finally, similarity in the seasonal patterns between the measured SIF (SIF_{FS2}) and GPP indicates the robustness of tower-based SIF measurement for tracking the seasonal variability of carbon assimilation (Figure 4). SIF_{FS2} and GPP levels were highest during the early growing season (May) and gradually decreased over time. On the other hand, the simulated SIF (SIF_{SC}) was highest during the summer, which coincided with the pattern of iPAR. The discrepancy in the seasonal patterns is likely to be determined by whether the SIF or GPP reflects seasonal variability in photosynthetic capacity (i.e., V_{cmax}). V_{cmax} is positively related to fluorescence yield under moderate to high light conditions (Frankenberg & Berry, 2018; van der Tol et al., 2014), and seasonally, the highest V_{cmax} is often reported during the early growing season (around May) for deciduous trees growing in temperate forests (Grassi et al., 2005; Wilson et al., 2000). Therefore, we presume that the observed seasonal patterns of SIF_{FS2} and GPP are more reliable than the seasonal pattern of SIF_{SC}, because V_{cmax} was set as a constant for the simulation (60 μmol m^{-2} s^{-1}) and light conditions would have a greater impact on SIF_{SC} than they would on SIF_{FS2}. This is demonstrated by a greater similarity in the seasonal pattern between SIF_{SC} and iPAR than between SIF_{FS2} and iPAR (Figure 4). Therefore, our findings suggest that prescribing V_{cmax} and its seasonality in the model is important for improving simulation accuracy.

5. Conclusion

SIF is widely accepted as a proxy for GPP due to its strong relationship with GPP observed from the field, airborne, and spaceborne measurements. Among these, tower-based SIF measurement enables continuous monitoring of SIF variation at a canopy or stand scale. Continuous measurement is particularly well suited to addressing physiological responses to rapidly changing environmental drivers, such as VPD (i.e., atmospheric dryness), which is highly variable during the day and is expected to increase with climate change. However, there is a potential challenge when using SIF to address the impact of environmental drivers: because of the strong and close relationship between SIF and aPAR, the response of SIF to environmental drivers might not be as evident as what we can learn from GPP. Our findings show that the SIF response to changing VPD, which is comparable to the response of GPP, can be replicated not only with high-frequency measurements (< hourly) but also with low-frequency measurements (> daily), if a proper definition of aPAR with a corresponding observational scale (canopy), such as $aPAR_{chl}$, is used. We also emphasize the importance of further research into methods for evaluating the fraction of aPAR at various observational scales to clarify the relationships between SIF, light conditions, and other environmental drivers.

Acknowledgments

XY acknowledges the support from the National Science Foundation (2005574 & 2023205). XY and RL acknowledge the support from The Future Investigators in NASA Earth and Space Science and Technology from the National Aeronautics and Space Administration (80NSSC22K1297).

References

Aiken, L. S., & West, S. G. (1991). Multiple regression: Testing and interpreting interactions. Sage Publications, Inc.

Bauer, D. J., & Curran, P. J. (2005). Probing interactions in fixed and multilevel regression: Inferential and graphical techniques. *Multivariate Behavioral Research, 40*(3), 373–400, https://doi.org/10.1207/s15327906mbr4003_5

Chan, S. (2011). *The Fate of Biogenic Hydrocarbons within a Forest Canopy: Field Observation and Model Results* [PhD Thesis, University of Virginia]. https://doi.org/10.18130/V3MV8J

Chang, C. Y., Guanter, L., Frankenberg, C., Köhler, P., Gu, L., Magney, T. S., Grossmann, K., & Sun, Y. (2020). Systematic assessment of retrieval methods for canopy far-red solar-induced chlorophyll fluorescence using high-frequency automated field spectroscopy. *Journal of Geophysical Research: Biogeosciences*, *125*(7), e2019JG005533. https://doi.org/10.1029/2019JG005533

Chaves, M. M., Flexas, J., & Pinheiro, C. (2009). Photosynthesis under drought and salt stress: Regulation mechanisms from whole plant to cell. *Annals of Botany*, *103*(4), 551–560. https://doi.org/10.1093/aob/mcn125

Cogliati, S., Rossini, M., Julitta, T., Meroni, M., Schickling, A., Burkart, A., Pinto, F., Rascher, U., & Colombo, R. (2015). Continuous and long-term measurements of reflectance and sun-induced chlorophyll fluorescence by using novel automated field spectroscopy systems. *Remote Sensing of Environment*, *164*, 270–281. https://doi.org/10.1016/j.rse.2015.03.027

Collatz, G. J., Ball, J. T., Grivet, C., & Berry, J. A. (1991). Physiological and environmental regulation of stomatal conductance, photosynthesis and transpiration: A model that includes a laminar boundary layer. *Agricultural and Forest Meteorology*, *54*(2), 107–136. https://doi.org/10.1016/0168-1923(91)90002-8

Du, S., Liu, L., Liu, X., Guo, J., Hu, J., Wang, S., & Zhang, Y. (2019). SIFSpec: Measuring Solar-Induced Chlorophyll Fluorescence Observations for Remote Sensing of Photosynthesis. *Sensors*, *19*(13), Article 13. https://doi.org/10.3390/s19133009

Flexas, J., Escalona, J. M., Evain, S., Gulías, J., Moya, I., Osmond, C. B., & Medrano, H. (2002). Steady-state chlorophyll fluorescence (Fs) measurements as a tool to follow variations of net CO2 assimilation and stomatal conductance during water-stress in C3 plants. *Physiologia Plantarum*, *114*(2), 231–240. https://doi.org/10.1034/j.1399-3054.2002.1140209.x

Flexas, J., Escalona, J. M., & Medrano, H. (1999). Water stress induces different levels of photosynthesis and electron transport rate regulation in grapevines. *Plant, Cell and Environment, 22*(1), 39–48. https://doi.org/10.1046/j.1365-3040.1999.00371.x

Frankenberg, C., Fisher, J. B., Worden, J., Badgley, G., Saatchi, S. S., Lee, J. E., Toon, G. C., Butz, A., Jung, M., Kuze, A., & Yokota, T. (2011). New global observations of the terrestrial carbon cycle from GOSAT: Patterns of plant fluorescence with gross primary productivity. Geophysical Research Letters, 38(17), L17706. https://doi.org/10.1029/2011GL048738

Frankenberg, C., & Berry, J. (2018). 3.10 - Solar Induced Chlorophyll Fluorescence: Origins, Relation to Photosynthesis and Retrieval. In S. Liang (Ed.), *Comprehensive Remote Sensing* (pp. 143–162). Elsevier. https://doi.org/10.1016/B978-0-12-409548-9.10632-3

Grassi, G., Vicinelli, E., Ponti, F., Cantoni, L., & Magnani, F. (2005). Seasonal and interannual variability of photosynthetic capacity in relation to leaf nitrogen in a deciduous forest plantation in northern Italy. *Tree Physiology*, *25*(3), 349–360. https://doi.org/10.1093/treephys/25.3.349

Grossiord, C., Buckley, T. N., Cernusak, L. A., Novick, K. A., Poulter, B., Siegwolf, R. T. W., Sperry, J. S., & McDowell, N. G. (2020). Plant responses to rising vapor pressure deficit. *New Phytologist*, *226*(6), 1550–1566. https://doi.org/10.1111/nph.16485

Grossmann, K., Frankenberg, C., Magney, T. S., Hurlock, S. C., Seibt, U., & Stutz, J. (2018). PhotoSpec: A new instrument to measure spatially distributed red and far-red Solar-Induced Chlorophyll Fluorescence. *Remote Sensing of Environment*, *216*, 311–327. https://doi.org/10.1016/j.rse.2018.07.002

Gu, L., Wood, J. D., Chang, C. Y.-Y., Sun, Y., & Riggs, J. S. (2019). Advancing Terrestrial Ecosystem Science With a Novel Automated Measurement System for Sun-Induced Chlorophyll Fluorescence for Integration With Eddy Covariance Flux Networks. *Journal of Geophysical Research: Biogeosciences*, *124*(1), 127–146. https://doi.org/10.1029/2018JG004742

Guanter, L., Rossini, M., Colombo, R., Meroni, M., Frankenberg, C., Lee, J.-E., & Joiner, J. (2013). Using field spectroscopy to assess the potential of statistical approaches for the retrieval of sun-induced chlorophyll fluorescence from ground and space. *Remote Sensing of Environment*, *133*, 52–61. https://doi.org/10.1016/j.rse.2013.01.017

Guanter, L., Zhang, Y., Jung, M., Joiner, J., Voigt, M., Berry, J. A., Frankenberg, C., Huete, A. R., Zarco-Tejada, P., Lee, J.-E., Moran, M. S., Ponce-Campos, G., Beer, C., Camps-Valls, G., Buchmann, N., Gianelle, D., Klumpp, K., Cescatti, A., Baker, J. M., & Griffis, T. J. (2014). Global and time-resolved monitoring of crop photosynthesis with chlorophyll fluorescence. *Proceedings of the National Academy of Sciences*, *111*(14), E1327–E1333. https://doi.org/10.1073/pnas.1320008111

Hanan, N. P., Burba, G., Verma, S. B., Berry, J. A., Suyker, A., & Walter-Shea, E. A. (2002). Inversion of net ecosystem CO2 flux measurements for estimation of canopy PAR absorption. *Global Change Biology*, *8*(6), 563–574. https://doi.org/10.1046/j.1365-2486.2002.00488.x

He, L., Magney, T., Dutta, D., Yin, Y., Köhler, P., Grossmann, K., Stutz, J., Dold, C., Hatfield, J., Guan, K., Peng, B., & Frankenberg, C. (2020). From the ground to space: Using solar-induced chlorophyll fluorescence to estimate crop productivity. *Geophysical Research Letters*, *47*(7), e2020GL087474. https://doi.org/10.1029/2020GL087474

Johnson, J. E. & Berry, J. A. (2021). The role of Cytochrome b_6f in the control of steady-state photosynthesis: a conceptual and quantitative model. *Photosynthesis Research, 148*, 101-136. https://doi.org/10.1007/s11120-021-00840-4

Johnson, P. O. & Fay, L. C. (1950). The Johnson-Neyman technique, its theory and application. *Psychometrika, 15*, 349–367. https://doi.org/10.1007/BF02288864

Kim, J., Ryu, Y., Dechant, B., Lee, H., Kim, H. S., Kornfeld, A., & Berry, J. A. (2021). Solar-induced chlorophyll fluorescence is non-linearly related to canopy photosynthesis in a temperate evergreen needleleaf forest during the fall transition. *Remote Sensing of Environment*, 258, 112362. https://doi.org/10.1016/j.rse.2021.112362

Lasslop, G., Reichstein, M., Papale, D., Richardson, A. D., Arneth, A., Barr, A., Stoy, P., & Wohlfahrt, G. (2010). Separation of net ecosystem exchange into assimilation and respiration using a light response curve approach: Critical issues and global evaluation. *Global Change Biology*, *16*(1), 187–208. https://doi.org/10.1111/j.1365-2486.2009.02041.x

Lawlor, D. W., & Cornic, G. (2002). Photosynthetic carbon assimilation and associated metabolism in relation to water deficits in higher plants. *Plant, Cell & Environment*, *25*(2), 275–294. https://doi.org/10.1046/j.0016-8025.2001.00814.x

Liu, L., Gudmundsson, L., Hauser, M., Qin, D., Li, S., & Seneviratne, S. I. (2020). Soil moisture dominates dryness stress on ecosystem production globally. *Nature Communications, 11*, 4892. https://doi.org/10.1038/s41467-020-18631-1

López, J., Way, D. A., & Sadok, W. (2021). Systemic effects of rising atmospheric vapor pressure deficit on plant physiology and productivity. *Global Change Biology*, *27*(9), 1704–1720. https://doi.org/10.1111/gcb.15548

Magney, T. S., Bowling, D. R., Logan, B. A., Grossmann, K., Stutz, J., Blanken, P. D., Burns, S. P., Cheng, R., Garcia, M. A., Köhler, P., Lopez, S., Parazoo, N. C., Raczka, B., Schimel, D., & Frankenberg, C. (2019). Mechanistic evidence for tracking the seasonality of photosynthesis with solar-induced fluorescence. *Proceedings of the National Academy of Sciences*, *116*(24), 11640–11645. https://doi.org/10.1073/pnas.1900278116

McDowell, N. G., Allen, C. D., Anderson-Teixeira, K., Aukema, B. H., Bond-Lamberty, B., Chini, L., Clark, J. S., Dietze, M., Grossiord, C., Hanbury-Brown, A., Hurtt, G. C., Jackson, R. B., Johnson, D. J., Kueppers, L., Lichstein, J. W., Ogle, K., Poulter, B., Pugh, T. A. M., Seidl, R., … Xu, C. (2020). Pervasive shifts in forest dynamics in a changing world. *Science*, *368*(6494), eaaz9463. https://doi.org/10.1126/science.aaz9463

McDowell, N. G., Sapes, G., Pivovaroff, A., Adams, H. D., Allen, C. D., Anderegg, W. R. L., Arend, M., Breshears, D. D., Brodribb, T., Choat, B., Cochard, H., De Cáceres, M., De Kauwe, M. G., Grossiord, C., Hammond, W. M., Hartmann, H., Hoch, G., Kahmen, A., Klein, T., … Xu, C. (2022). Mechanisms of woody-plant mortality under rising drought, CO2 and vapour pressure deficit. *Nature Reviews Earth & Environment*, *3*(5), Article 5. https://doi.org/10.1038/s43017-022-00272-1

Miao, G., Guan, K., Yang, X., Bernacchi, C. J., Berry, J. A., DeLucia, E. H., Wu, J., Moore, C. E., Meacham, K., Cai, Y., Peng, B., Kimm, H., & Masters, M. D. (2018). Sun-Induced Chlorophyll Fluorescence, Photosynthesis, and Light Use Efficiency of a Soybean Field from Seasonally Continuous Measurements. *Journal of Geophysical Research: Biogeosciences*, *123*(2), 610–623. https://doi.org/10.1002/2017JG004180

Novick, K. A., Ficklin, D. L., Stoy, P. C., Williams, C. A., Bohrer, G., Oishi, A. C., Papuga, S. A., Blanken, P. D., Noormets, A., Sulman, B. N., Scott, R. L., Wang, L., & Phillips, R. P. (2016a). The increasing importance of atmospheric demand for ecosystem water and carbon fluxes. *Nature Climate Change*, *6*(11), Article 11. https://doi.org/10.1038/nclimate3114

Novick, K. A., Miniat, C. F., & Vose, J. M. (2016b). Drought limitations to leaf-level gas exchange: Results from a model linking stomatal optimization and cohesion-tension theory. *Plant Cell Environ.*, *39*(3), 583–596.

Ogutu, B. O., & Dash, J. (2013). An algorithm to derive the fraction of photosynthetically active radiation absorbed by photosynthetic elements of the canopy (FAPARps) from eddy covariance flux tower data. *New Phytologist*, *197*(2), 511–523. https://doi.org/10.1111/nph.12039

Oren, R., Sperry, J. S., Katul, G. G., Pataki, D. E., Ewers, B. E., Phillips, N., & Schäfer, K. V. R. (1999). Survey and synthesis of intra- and interspecific variation in stomatal sensitivity to vapour pressure deficit. *Plant, Cell & Environment*, *22*(12), 1515–1526. https://doi.org/10.1046/j.1365-3040.1999.00513.x

Parazoo, N. C., Magney, T., Norton, A., Raczka, B., Bacour, C., Maignan, F., Baker, I., Zhang, Y., Qiu, B., Shi, M., MacBean, N., Bowling, D. R., Burns, S. P., Blanken, P. D., Stutz, J., Grossmann, K., & Frankenberg, C. (2020). Wide discrepancies in the magnitude and direction of modeled solar-induced chlorophyll fluorescence in response to light conditions. *Biogeosciences*, *17*(13), 3733–3755. https://doi.org/10.5194/bg-17-3733-2020

Paul-Limoges, E., Damm, A., Hueni, A., Liebisch, F., Eugster, W., Schaepman, M. E., & Buchmann, N. (2018). Effect of environmental conditions on sun-induced fluorescence in a mixed forest and a cropland. *Remote Sensing of Environment*, *219*, 310–323. https://doi.org/10.1016/j.rse.2018.10.018

Porcar-Castell, A. (2011). A high-resolution portrait of the annual dynamics of photochemical and non-photochemical quenching in needles of Pinus sylvestris. *Physiologia Plantarum, 143*(2), 139-153. https://doi.org/10.1111/j.1399-3054.2011.01488.x

Porcar-Castell, A., Malenovský, Z., Magney, T., Van Wittenberghe, S., Fernández-Marín, B., Maignan, F., et al. (2021). Chlorophyll a fluorescence illuminates a path connecting plant molecular biology to Earth-system science. *Nature Plants, 7*(8), 998–1009. https://doi.org/10.1038/s41477-021-00980-4

Porcar-Castell, A., Tyystjärvi, E., Atherton, J., van der Tol, C., Flexas, J., Pfündel, E. E., Moreno, J., Frankenberg, C., & Berry, J. A. (2014). Linking chlorophyll a fluorescence to photosynthesis for remote sensing applications: Mechanisms and challenges. *Journal of Experimental Botany*, *65*(15), 4065–4095. https://doi.org/10.1093/jxb/eru191

Sun, Y., Frankenberg, C., Wood, J. D., Schimel, D. S., Jung, M., Guanter, L., Drewry, D. T., Verma, M., Porcar-Castell, A., Griffis, T. J., Gu, L., Magney, T. S., Köhler, P., Evans, B., & Yuen, K. (2017). OCO-2 advances photosynthesis observation from space via solar-induced chlorophyll fluorescence. *Science*, *358*(6360), eaam5747. https://doi.org/10.1126/science.aam5747

Stovall, A. E., Masters, B., Fatoyinbo, L., & Yang, X. (2021). TLSLEAF: automatic leaf angle estimates from single-scan terrestrial laser scanning. *New Phytologist, 232*(4). https://doi.org/10.1111/nph.17548

Tezara, W., Mitchell, V. J., Driscoll, S. D., & Lawlor, D. W. (1999). Water stress inhibits plant photosynthesis by decreasing coupling factor and ATP. *Nature*, *401*(6756), Article 6756. https://doi.org/10.1038/44842 van der Tol, C., Berry, J. A., Campbell, P. K. E., & Rascher, U. (2014). Models of fluorescence and photosynthesis for interpreting measurements of solar-induced chlorophyll fluorescence. *Journal of Geophysical Research: Biogeosciences*, *119*(12), 2312–2327. https://doi.org/10.1002/2014JG002713

van der Tol, C., Verhoef, W., & Rosema, A. (2009). A model for chlorophyll fluorescence and photosynthesis at leaf scale. *Agricultural and Forest Meteorology*, *149*(1), 96–105. https://doi.org/10.1016/j.agrformet.2008.07.007

Verhoef, A., McNaugthton, K.G., & Jacobs, A.F.G. (1997). A parameterization of momentum roughness length and displacement height for a wide range of canopy densities. *Hydrology and Earth System Sciences, 1*, 81-91. https://doi.org/10.5194/hess-1-81-1997

Verrelst, J., Rivera, J. P., van der Tol, C., Magnani, F., Mohammed, G., & Moreno, J. (2015). Global sensitivity analysis of the SCOPE model: What drives simulated canopy-leaving sun-induced fluorescence? *Remote Sensing of Environment*, *166*, 8–21. https://doi.org/10.1016/j.rse.2015.06.002

Wang, X., Qiu, B., Li, W., & Zhang, Q. (2019). Impacts of drought and heatwave on the terrestrial ecosystem in China as revealed by satellite solar-induced chlorophyll fluorescence. *Science of The Total Environment*, *693*, 133627. https://doi.org/10.1016/j.scitotenv.2019.133627

Weis, E., & Berry, J. A. (1987). Quantum efficiency of Photosystem II in relation to ‘energy’-dependent quenching of chlorophyll fluorescence. *Biochimica et Biophysica Acta (BBA) - Bioenergetics*, *894*(2), 198–208. https://doi.org/10.1016/0005-2728(87)90190-3

Wilson, K. B., Baldocchi, D. D., & Hanson, P. J. (2000). Spatial and seasonal variability of photosynthetic parameters and their relationship to leaf nitrogen in a deciduous forest. *Tree Physiology*, *20*(9), 565–578. https://doi.org/10.1093/treephys/20.9.565

Wutzler, T., Lucas-Moffat, A., Migliavacca, M., Knauer, J., Sickel, K., Šigut, L., Menzer, O., & Reichstein, M. (2018). Basic and extensible post-processing of eddy covariance flux data with REddyProc. *Biogeosciences*, *15*(16), 5015–5030. https://doi.org/10.5194/bg-15-5015-2018

Yang, X., Li, R., Jablonski, A., Stovall, A., Kim, J., Yi, K., Ma, Y., Beverly, D., Phillips, R., Novick, K., Xu, X., & Lerdau, M. (2023). Leaf angle as a leaf and canopy trait: Rejuvenating its role in ecology with new technology. *Ecology Letters, 26*(6), 1005–1020. https://doi.org/10.1111/ele.14215

Yang, X., Shi, H., Stovall, A., Guan, K., Miao, G., Zhang, Y., Zhang, Y., Xiao, X., Ryu, Y., & Lee, J.-E. (2018). FluoSpec 2—An automated field spectroscopy system to monitor canopy solar-induced fluorescence. *Sensors*, *18*(7), Article 7. https://doi.org/10.3390/s18072063

Yang, X., Tang, J., Mustard, J. F., Lee, J.-E., Rossini, M., Joiner, J., Munger, J. W., Kornfeld, A., & Richardson, A. D. (2015). Solar-induced chlorophyll fluorescence that correlates with canopy photosynthesis on diurnal and seasonal scales in a temperate deciduous forest. *Geophysical Research Letters*, *42*(8), 2977–2987. https://doi.org/10.1002/2015GL063201

Yi, K., Maxwell, J. T., Wenzel, M. K., Roman, D. T., Sauer, P. E., Phillips, R. P., & Novick, K. A. (2019). Linking variation in intrinsic water-use efficiency to isohydricity: A comparison at multiple spatiotemporal scales. *New Phytologist*, *221*(1), 195–208. https://doi.org/10.1111/nph.15384

Yin, X., Harbinson, J., & Struik, P.C. (2006). Mathematical review of literature to assess alternative electron transports and interphotosystem excitation partitioning of steady-state C3 photosynthesis under limiting light. *Plant, Cell & Environment, 29*(9), 1771-1782. https://doi.org/10.1111/j.1365-3040.2006.01554.x

Yin, X & Struik, P.C. (2012). Mathematical review of the energy transduction stoichiometries of C4 leaf photosynthesis under limiting light. *Plant, Cell & Environment, 35*(7), 1299-1312. https://doi.org/10.1111/j.1365-3040.2012.02490.x

Zeng, Y., Badgley, G., Dechant, B., Ryu, Y., Chen, M., & Berry, J. A. (2019). A practical approach for estimating the escape ratio of near-infrared solar-induced chlorophyll fluorescence. *Remote Sensing of Environment*, *232*, 111209. https://doi.org/10.1016/j.rse.2019.05.028

Zhang, Y., Guanter, L., Berry, J. A., van der Tol, C., Yang, X., Tang, J., & Zhang, F. (2016a). Model-based analysis of the relationship between sun-induced chlorophyll fluorescence and gross primary production for remote sensing applications. *Remote Sensing of Environment*, *187*, 145–155. https://doi.org/10.1016/j.rse.2016.10.016

Zhang, Y., Xiao, X., Jin, C., Dong, J., Zhou, S., Wagle, P., Joiner, J., Zhang, Y., Zhang, G., Qin, Y., Wang, J., & Moore, B. (2016b). Consistency between sun-induced chlorophyll fluorescence and gross primary production of vegetation in North America. Remote Sensing of Environment, 183, 154-169. https://doi.org/10.1016/j.rse.2016.05.015

Zhang, Y., Xiao, X., Zhang, Y., Wolf, S., Zhou, S., Joiner, J., Guanter, L., Verma, M., Sun, Y., Yang, X., Paul-Limoges, E., Gough, C. M., Wohlfahrt, G., Gioli, B., van der Tol, C., Yann, N., Lund, M., & de Grandcourt, A. (2018). On the relationship between sub-daily instantaneous and daily total gross primary production: Implications for interpreting satellite-based SIF retrievals. *Remote Sensing of Environment*, *205*, 276–289. https://doi.org/10.1016/j.rse.2017.12.009

Zhang, Z., Zhang, Y., Zhang, Y., Gobron, N., Frankenberg, C., Wang, S., & Li, Z. (2020). The potential of satellite FPAR product for GPP estimation: An indirect evaluation using solar-induced chlorophyll fluorescence. *Remote Sensing of Environment*, *240*, 111686. https://doi.org/10.1016/j.rse.2020.111686

List of Figure Captions

Figure 1. The design of instrument setup (Fluospec 2) at the study site (Virginia Forest Research Facility, a) and a sample thermal image taken at 13:00 EST on August 8, 2019 at the top platform of a flux tower near the SIF sensors (b). Fluospec 2 is composed of a SIF spectrometer, a computer for system operation (Raspberry Pi), and an optical shutter. The system is enclosed in a thermostatic box, with the temperature inside the enclosure set at 25°C, and resides inside a research hut. The ends of optical cables measuring irradiance and canopy radiance are installed on the top platform of a flux tower (40 m tall). Note that the field of view (FOV) of the optical fibers (25 degree) is smaller than the FOV of the thermal camera (45 degree). Thus, SIF is observed for a smaller area than appears in the thermal image in panel b.

Figure 2. An example of data collected by Fluospec 2 at noon on June 14, 2019. Irradiance (orange in panel a) was collected by an upward-looking cosine corrector, and radiance (blue in panel a) was collected by an optical fiber pointing to the target tree canopy. Reflectance (b) was calculated by dividing radiance by irradiance and multiplying by π. The shaded area in green in panel b indicates the fitting window (759.5-761.5 nm) used for O_2A retrieval (Chang et al., 2020).

Figure 3. Example of data transformation of SIF, GPP, and aPAR for different levels of VPD (grouped based on the quartiles of the VPD distribution, Q1: 0.0 - 1.3 kPa, Q2: 1.3 - 1.9 kPa, Q3: 1.9 - 2.5 kPa, and Q4: 2.5 - 3.7 kPa). The non-linear power functions for the SIF-aPAR (SIF = $a \cdot \mathrm{aPAR}^b$) and GPP-aPAR relationships (GPP = $a \cdot \mathrm{aPAR}^b$) were transformed by applying natural

log to both sides of the equation (e.g., ln (SIF) = ln a + b·ln(aPAR), where b is the slope, and ln a is the intercept in the transformed relationships.)

Figure 4. Monthly mean diurnal patterns of GPP estimated from the eddy covariance method, SIF measured by Fluospec 2 (SIF_{FS2}), SIF simulated by SCOPE (SIF_{SC}), and environmental variables including incident PAR (iPAR), vapor pressure deficit (VPD), and air temperature (T_a), and their monthly mean between 10 am to 2 pm. Error bars represent standard deviations.

Figure 5. Relationships between incident PAR (iPAR) and different absorbed PAR (aPAR) metrics. Gray dashed lines indicate a 1:1 line. Red solid lines indicate linear regression fit.

Figure 6. Effect of VPD on GPP-aPAR relationship at hourly scale. The top row (a-d) shows the results of Johnson-Neyman analysis, identifying the range of aPAR metrics where the influence of VPD on GPP-aPAR regression is significant ($P < 0.05$, shaded in green). The thicker horizontal lines at 0 in Johnson-Neyman plots indicate the observed range of aPAR metrics. The middle row (e-h) shows scatter plots of log-transformed and GPP and aPAR metrics. The bottom row (i-l) shows the results of Simple slopes analysis, illustrating GPP-aPAR regressions held at three VPD levels: mean VPD, mean VPD plus 1.5 times standard deviation, and mean VPD minus 1.5 times standard deviation. Note that confidence intervals are illustrated in gray around the fitted lines (i-l) but are barely visible because they are very narrow, especially under high aPAR. Slope and standard error (SE) values are presented (i-l), and the text colors match the colors of the fitted lines.

Figure 7. Effect of VPD on SIF-aPAR relationship at hourly scale. The top row (a-e) shows the results of Johnson-Neyman analysis, identifying the range of aPAR metrics where the influence of VPD on SIF-aPAR regression is significant ($P < 0.05$, shaded in green). The thicker horizontal lines at 0 in Johnson-Neyman plots indicate the observed range of aPAR metrics. The middle row (f-j) shows scatter plots of log-transformed and SIF and aPAR metrics. The bottom row (k-o) shows the results of Simple slopes analysis, illustrating SIF-aPAR regressions held at three VPD levels: mean VPD, mean VPD plus 1.5 times standard deviation, and mean VPD minus 1.5 times standard deviation. Note that confidence intervals are illustrated in gray around the fitted lines (k-o) but are barely visible because they are very narrow, especially under high aPAR. Slope and standard error (SE) values are presented (k-o), and the text colors match the colors of the fitted lines.

Figure 8. Effect of VPD on SIF-aPAR relationship at daily scale. The top row (a-e) shows the results of Johnson-Neyman analysis, identifying the range of aPAR metrics where the influence of VPD on SIF-aPAR regression is significant ($P < 0.05$, shaded in green). The thicker horizontal lines at 0 in Johnson-Neyman plots indicate the observed range of aPAR metrics. The middle row (f-j) shows scatter plots of log-transformed and SIF and aPAR metrics. The bottom row (k-o) shows the results of the Simple slopes analysis, illustrating SIF-aPAR regressions held at three VPD levels: mean VPD, mean VPD plus 1.5 times standard deviation, and mean VPD minus 1.5 times standard deviation. Note that confidence intervals are illustrated in gray around the fitted lines (k-o) but are barely visible because they are very narrow, especially under high aPAR.

Slope and standard error (SE) values are presented (k-o), and the text colors match the colors of the fitted lines.

Figure 9. Non-linear relationships between GPP and SIF measured by Fluospec 2 at different levels of VPD (grouped based on the quartiles of the VPD distribution, Q1: 0.0 - 1.3 kPa, Q2: 1.3 - 1.9 kPa, Q3: 1.9 - 2.5 kPa, and Q4: 2.5 - 3.7 kPa) at hourly (a, b, c) and daily scales (d, e, f). The GPP-SIF relationships were fitted using a power function (i.e., GPP = $k \times \text{SIF}^{a}$). Error bars represent standard errors of means (95% confidence). Coefficient k (b & e) or exponent a (c & f) marked with different letters are significantly different ($p < 0.05$).

Figure 10. Variations of quantum yields (Φ_P: photochemistry, Φ_F: fluorescence, Φ_N: non-photochemical quenching, Φ_D: non-radiative decay) with changing aPAR simulated by SCOPE using two different modes (i.e., Moderate and SM Stress modes) across different VPD levels (grouped based on the quartiles of the VPD distribution, Q1: 0.0 - 1.3 kPa, Q2: 1.3 - 1.9 kPa, Q3: 1.9 - 2.5 kPa, and Q4: 2.5 - 3.7 kPa).